Photoemission studies of the electronic properties of the Ce/Fe(100) and Ce/Fe(110) interfaces: Formation of a strongly hybridized cerium phase

B. Kierren, F. Bertran, T. Gourieux, N. Witkowski, and D. Malterre
Laboratoire de Physique du Solide, Université Henri Poincaré, Nancy I, Boîte Postale 239, F-54506 Vandœuvre-lès-Nancy, France*

G. Krill
Laboratoire pour l'Utilisation du Rayonnement Electromagnétique, Université Paris-Sud, F-91405 Orsay Cedex, France
(Received 17 July 1995; revised manuscript received 28 September 1995)

The electronic structure of very thin cerium films deposited on Fe(100) and Fe(110) surfaces has been investigated by Ce $3d$ photoemission. The cerium layers were disordered and the growth was mainly of a two-dimensional nature. Ce $3d$ photoemission experiments have revealed the formation of a strongly hybridized cerium phase at the interface with iron for both orientations. Obviously, photoemission spectra contain a contribution from bulk cerium and a contribution from the surface where hybridization is reduced. By covering cerium layers with three layers of samarium we have been able to suppress the influence of the surface and we have obtained the contribution from each atomic layer. The electronic structures of these atomic layers are very different from each other and the corresponding photoemission spectra have been simulated with the Gunnarsson-Schönhammer model.

I. INTRODUCTION

Cerium is a very particular rare-earth element exhibiting an isostructural phase transition from the γ-Ce phase toward α-Ce at about 7 kbar and room temperature.[1] This transition is accompanied by a 7% reduction of the lattice parameter and by an increase in the hybridization of the $4f$ states with conduction band. Two opposite models are generally proposed to explain this transition and to describe the cerium ground-state properties. The first one treats $4f$ states with a band formalism[2–4] and considers γ-Ce $\rightarrow$ α-Ce as a Mott transition:[5] the $4f$ electrons are well localized in γ-Ce and they acquire an itinerant character when the transition toward the α-Ce phase occurs without any significant change of the $4f$ occupation number. On the other hand, a many-body approach in the Anderson model framework[6,7] considers the $4f$ states as localized states hybridized with delocalized conduction states. This model provides a satisfactory description as well of the ground-state properties as of the dynamical behaviors (such as high-energy spectroscopies).[8] Nevertheless, this phenomenological treatment does not take into account the interactions between neighboring cerium atoms and the $4f$-band picture may be more accurate if these interactions become strong. In metallic Ce-based systems, the character of the $4f$ states depends on the hybridization between Ce $4f$ and itinerant states of the other elements. The strongly and weakly hybridized Ce electronic configurations in compounds are usually characterized by α-like and γ-like terms, respectively (by analogy with the electronic configuration of cerium metal).

Photoemission is a suitable technique to study the electronic properties of Ce-based systems and to test the predictions of these two different theoretical approaches. However, photoemission spectroscopy is a surface sensitive technique and the contribution from the surface atomic layer to the total photoemission spectrum is important. In the case of Sm, Eu, Tm, or Yb-based compounds, it has been shown that a valence transition could occur at the surface.[9–12] This behavior generates difficulties in the interpretation of the photoemission results that are not directly representative of the bulk electronic structure.

In the case of cerium, this point has been recently addressed and it is still discussed. A theoretical study in the $4f$-band formalism has predicted that the surface of α-Ce should be γ-like.[13] This result has been experimentally observed on some α-like Ce compounds[14,15] and confirmed on α-Ce,[16] which have γ-like surfaces. These authors noticed that it is necessary to take into account the electronic structure modification at the surface of strongly hybridized Ce-based compounds in order to perform a correct analysis of the photoemission spectra. In that case, the bulk cerium atoms appear to be more strongly hybridized than it was considered previously.

However, it has been shown that some systems do not exhibit surface hybridization reduction. Tang, Lawrence, and Hemminger have obtained an epitaxial compound ($CePt_{2.23}$) by deposition of Ce on a Pt(111) surface and 770-K annealings.[17] Photoemission results indicate that this compound is α-like in the bulk and also at the surface. This behavior is interpreted by the fact that the surface is Pt enriched and there are then few cerium atoms in contact with the free surface. Finally, another study demonstrates that one could obtain one atomic α-Ce layer at the surface. By depositing cerium on a W(110) surface, Gu *et al.* have evidenced a γ-Ce $\rightarrow$ α-Ce transition during the first atomic layer formation.[18] This transition is due to the increase of the layer compactness, which leads to the decrease of the lattice parameter. In that case, the hybridization strength increase due to the Ce-Ce interactions overbalances the surface effect.

Then this surface hybridization reduction is not a general rule and, since the surface effect is not well understood, this subject needs further studies. When the surface hybridization

reduction is well established, one needs an exact knowledge of the depth affected by this reduction to interpret the photoemission spectra. In that way, L. Braicovich *et al.* have recently separated α-like bulk and γ-like surface contributions from Ce 3*d* photoemission spectra of various Ce-Rh compounds.[19] They have estimated that the hybridization is reduced for the two atomic layers under the surface. In this study, as in the previous ones, which have taken numerically into account a γ-like surface contribution, an attenuation coefficient or an electron inelastic-math-free-path (IMFP) has been arbitrarily chosen. The choice of this value is rather difficult and may be greatly responsible for uncertainties. Consequently, some aims of our work are as follows: to obtain photoemission spectra of α-like bulk cerium directly without numerical treatment, to give an estimation of the hybridization reduction depth, and to study separately the electronic structures of the single atomic layers in some Ce films. To address these questions, scraped polycrystalline sample are not suitable and it is necessary to work on well-characterized systems. We have deposited cerium on Fe(100) and Fe(110) surfaces since no interdiffusion occurs at the interfaces in Ce/Fe multilayers.[20] Moreover, it has been shown that cerium exhibits very unusual electronic and magnetic properties in these multilayers. At the interfaces, cerium is α-like and magnetic circular x-ray dichroism (MCXD) experiments on Ce $L_{2,3}$ edges have revealed that Ce atoms carry a 5*d* magnetic moment, which is antiferromagnetically coupled to the Fe 3*d* moment.[21] Finally, recent MCXD experiments on Ce $M_{4,5}$ edges have shown the existence of a 4*f* magnetic moment.[22] This result points out the problem of the coexistence of a localized 4*f* magnetic moment with the partial delocalization of these states. In that way, a precise knowledge of the electronic structure of the cerium layers at the interface is of great importance.

The paper is organized as follows: we shall characterize the growth mode (Sec. III A) and the crystallographic structure (Sec. III B) of the Ce films. Core-level photemission results for various film thicknesses will be presented in Sec. III C. Next, we shall show that it is possible to eliminate the surface contribution to the photoemission spectra by covering cerium films with samarium overlayers (Sec. IV). The surface effect will then be discussed and we shall extract the contribution from each atomic layers of the cerium films. These basic spectra will finally be simulated in the Gunnarsson-Schönhammer model.

II. EXPERIMENTAL PROCEDURE

Ultrathin films of cerium were evaporated on (100)- and (110)-oriented monocrystalline iron substrates. To avoid sulfur or nitrogen contamination frequently encountered with monocrystalline massive iron, we used epitaxial 3500-Å-thick iron films as substrates. The Fe(100) and Fe(110) were grown respectively on MgO(100) (Ref. 23) and $Al_2O_3(11\bar{2}0)$ (Ref. 24) covered with an iridium buffer. These substrates were prepared in a molecular-beam epitaxy (MBE) apparatus other than cerium depositions. The iron substrates were therefore covered with a 20-Å-thick iridium film to protect them during the transfer from the first apparatus to the other. This protection was removed by ionic etching and surface recrystallization was achieved by 825-K annealing for 10 min. Before each deposition, the preceding cerium film was removed in the same way and then surface cleanliness was checked with Auger spectroscopy. Recrystallization was verified with reflection high energy electron diffraction (RHEED).

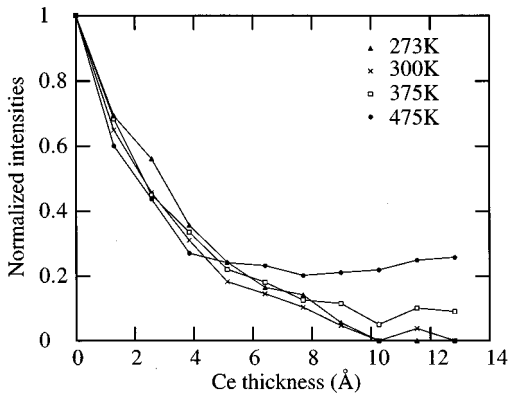

FIG. 1. Dependence of the Fe(*MVV*) Auger transition intensity on cerium thickness for different substrate temperatures. For temperatures smaller than 375 K, the iron signal vanishes for cerium thicknesses larger than 10 Å. Intensities are normalized to unity for bare substrate.

Our experimental setup consists of a MBE chamber with RHEED and Auger spectroscopy equipment that is connected to a photoemission chamber VG ESCALAB MK II. Cerium of 99.9% purity was evaporated from a tungsten crucible heated by Joule effect and samarium was sublimated from an effusion cell at 765 K. The film thicknesses were measured with quartz microbalances calibrated from Auger intensity measurements in the case of cerium evaporations as we will see in Sec. III A and the evaporation rates were within the 1–2-Å min^{-1} range. In the case of samarium evaporations, the quartz microbalance was calibrated from depositions on Co(0001).[25] The base pressure in all the apparatus was about 4×10^{-11} hPa and the pressure never exceeded 2×10^{-10} hPa during evaporations.

Auger spectra were recorded in the derivative mode with a 3-V peak-to-peak modulation and a primary electron beam of 2 μA. Photoemission spectra were obtained with Mg $K\alpha$ radiation ($h\nu$=1253.6 eV) and recorded in the constant ΔE mode with a pass energy of 20 eV leading to an experimental resolution of about 1 eV. The contributions due to the $K\alpha_2$ and $K\alpha_3$ radiations were numerically subtracted from all the presented spectra.

III. ROOM-TEMPERATURE INTERFACE PROPERTIES

A. Auger results

A precedent study[29] showed the possibility of obtaining an epitaxial Ce_2Fe_{17} compound by deposition of cerium on Fe(100) and reactive diffusion process. The aim of the present work is the study of the behavior of the Ce/Fe(100) and Ce/Fe(110) interfaces at room temperature. We have first to know the growth mode and, more particularly, to determine if an interdiffusion process occurs.

For this purpose, we recorded for different temperatures the dependence of the Fe(*MVV*) Auger transition intensity on the cerium deposited quantity (Fig. 1) in order to deter-

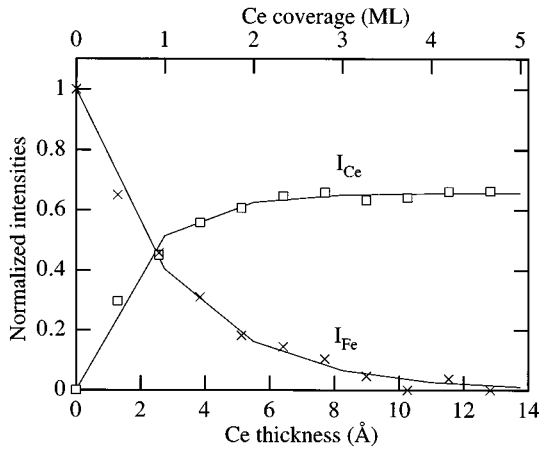

FIG. 2. Thickness dependence of the Fe(MVV) and Ce(NVV) Auger transition intensities and layer-by-layer growth model (solid line). Intensities are normalized to unity for iron intensity on bare substrate.

mine the temperature range where interdiffusion occurs. For the 275- and 300-K measurements, the iron signal disappears for cerium film thicknesses greater than 10 Å. This behavior suggests a uniform coverage of the iron surface and indicates that, for these temperatures, no noticeable interdiffusion (which would lead to the persistence of the iron signal) occurs. We will see later that by fitting a layer-by-layer growth model to the experimental data, we can conclude a two-dimensional growth. For higher temperatures (375 and 475 K), the nonzero iron intensity for cerium thicknesses greater than 10 Å demonstrates that interdiffusion occurs. This signal is due to iron atoms that have interdiffused in the cerium layer. One should notice that asymptotic value reached by iron intensity for a large cerium thickness depends on the temperature, which means that the higher the temperature, the larger the interdiffusion. As a consequence, we have carried out cerium deposition at room temperature to avoid interdiffusion except films with samarium coverage (Sec. IV A), which were elaborated at 130 K.

The evolution of the Auger intensities at room temperature can give information about the cerium film growth mode. We have reported (Fig. 2) the Auger intensities I_{Ce} and I_{Fe} as a function of the cerium thickness. A model of layer-by-layer growth has been fitted to the experimental data. In this model, the iron and cerium intensities for a deposit of n complete monolayers of cerium ($n \geqslant 1$) are given by

$$I_{Fe}^{n} = I_{Fe}^{0} \exp(-nd/\lambda_{Fe}\cos 42°), \tag{3.1}$$

$$I_{Ce}^{n} = I_{Ce}^{1} \sum_{m=1}^{n-1} \exp(-md/\lambda_{Ce}\cos 42°), \tag{3.2}$$

where λ_{Fe} and λ_{Ce} are the electron attenuation lengths (AL's) at the energies of the Fe(MVV) and Ce(NVV) transitions (47 and 90 eV, respectively), d is the equivalent thickness of one atomic layer of Ce (see below), and cos42° accounts for the detection angle.

The best agreement with experimental data is obtained for $\lambda_{Fe} = 4.1 \pm 0.3$ Å and $\lambda_{Ce} = 2.4 \pm 0.3$ Å and the corresponding result is presented in Fig. 2. These values seem weak in comparison with those observed in many materials and are in contradiction with the universal behavior proposed by Seah and Dench, which suggests a minimum AL around 40 eV.[26] Very few experimental data are available for rare earths and it should be noticed that AL's involved in the above expressions are always 15–30% (even more for low electron energies and in the case of high atomic number elements) smaller than the electron IMFP's that are usually calculated.[27] Moreover, it has been shown that the IMFP behavior at low energy is greatly material dependent. The calculated IMFP minimum could lie between 30 eV (Si) and 140 eV (Au) (Ref. 28) but no calculations are available for rare earths. This result demonstrates that the energy dependence of Seah and Dench is not a general rule. Therefore, the contradiction with the ''universal'' behavior does not invalidate the experimental AL values we obtain. The thickness dependence of the Auger intensities allows us to exclude a multilayer growth at least for thicknesses smaller than 4–5 monolayers (ML). The multilayer growth would lead to a larger Fe (smaller Ce) intensity than actually observed. However, for larger thicknesses (>5 ML), the Fe intensity vanishes so that the experimental data become consistent with several growth modes. But this behavior is not prejudicial for our photoemission analysis as discussed in Sec. IV.

In the case of a layer-by-layer growth, the positions corresponding to the formation of the complete cerium monolayers allow the calibration of the thicknesses measured by the quartz microbalance. In a previous study devoted to the 650 °C depositions,[29] we arbitrarily considered that the equivalent thickness of one cerium monolayer was that of a γ-Ce (100) plane, i.e., 2.5 Å. In the present work, as we will see later, RHEED experiments have shown that cerium films do not exhibit a long-range order and we do not have information about their structure. Thus, we believe that it would be better to consider that one monolayer contains 8×10^{14} atoms cm^{-2}, which is an average of the two dense planes (100) and (110) of γ-Ce phase. Assuming that the thin-film density is that of massive γ-Ce, an equivalent thickness of 2.75 Å can be obtained for one monolayer. This value constitutes the calibration for the quartz microbalance from which the thicknesses of all cerium films are deduced. For simplicity, we have not taken into account the 7% decrease of the lattice parameter that occurs at the γ-Ce $\rightarrow$ α-Ce transition.[1]

B. Structural properties

When cerium is deposited at room temperature, the intensity of Fe(100) RHEED patterns decreases rapidly for thicknesses greater than one monolayer and these patterns totally disappear above two monolayers. We then observe a diffuse background characteristic of the absence of long-range order. We can then conclude that there is the formation of a disordered cerium phase, which confirms the results of Klose *et al.*,[20] who observed that cerium is amorphous in Ce/Fe multilayers. Moreover, for several rare-earth/iron systems [Gd/Fe(100),[30,31] Tb/Fe(100) and Dy/Fe(100),[32] Sm/Fe(100) (Ref. 33)] low-energy electron diffraction experiments revealed the growth of disordered rare earth.

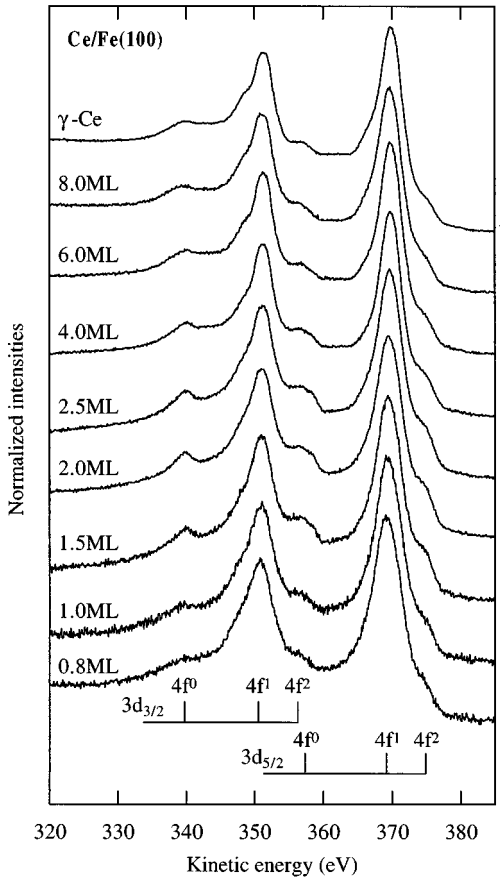

FIG. 3. Ce 3*d* photoemission spectra for different cerium thicknesses on Fe(100). All spectra are normalized at the $4f^1$ feature intensity at 369 eV.

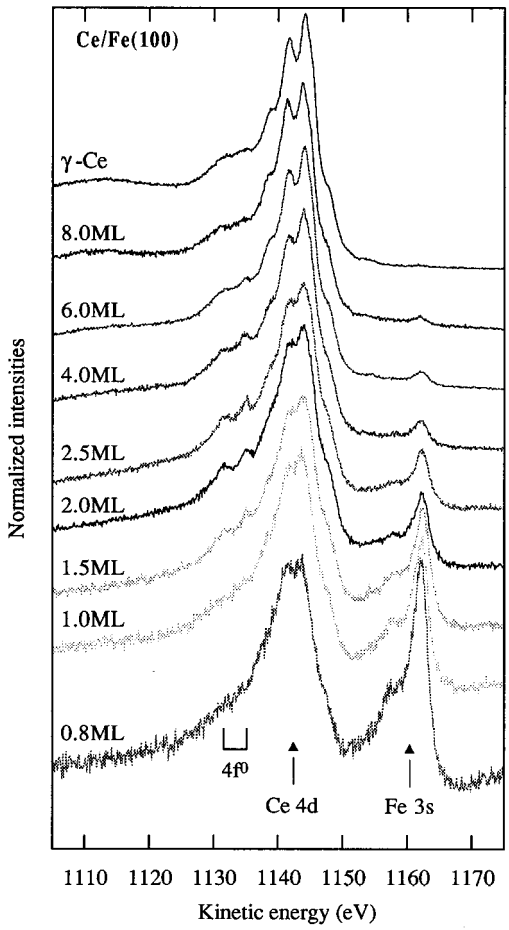

FIG. 4. Ce 4*d* and Fe 3*s* photoemission spectra for different cerium thicknesses on Fe(100). All spectra are normalized at the main Ce 4*d* feature intensity at 1144 eV.

C. Photoemission results

Dependence of Ce 3*d* photoemission spectra on a cerium deposited quantity is presented in Fig. 3. The different features are labeled from the dominating 4*f* electronic configuration in the final state. Moreover, each one of these transitions is split by spin-orbit interaction within 3*d* states. The main feature is always the $4f^1$ one while the $4f^0$ and $4f^2$ features are satellites, intensities of which depend on hybridization strength and on the configuration mixing in the initial state. The $4f^0$ feature corresponds to transitions toward nearly pure $4f^0$ states and then provides an estimation of this configuration weight in the initial state (i.e., a measurement of the 4*f* state occupation number n_f since the intensity of the $4f^0$ feature is related to $1-n_f$). The $4f^2$ feature corresponds to transitions toward states associated with a mixture of $4f^1$ and $4f^2$ configurations in the final state and its intensity is directly related to the hybridization strength.[34]

Three different steps in the evolution of the Ce 3*d* photoemission spectra may be distinguished. Firstly, for thicknesses lower than one monolayer, the $4f^0$ feature intensity is very small and compares with that observed on the weakly hybridized γ-Ce phase. For larger thicknesses, the $4f^0$ intensity strongly increases and reaches a maximum for a 2.5 ML film. This result unambiguously demonstrates the formation of a strongly hybridized cerium phase. Finally, the $4f^0$ intensity progressively decreases and for large thicknesses the spectrum characteristic of γ-Ce (Ref. 35) is observed. The reference spectra shown in Fig. 3 were obtained for a 50-Å film on iron substrate. One can assume that for such a thick film, cerium, which contributes to the photoemission signal, does not feel the iron influence.

One should notice that in the case of thicknesses lower than 4 ML, photoemission spectra contain several contributions associated with distinct electronic configurations of the different layers. Therefore, the experimental spectra only represent the mean electronic configuration of the film. We will discuss this problem in Sec. IV.

We have also recorded the Ce 4*d* and Fe 3*s* photoemission spectra evolution (Fig. 4), which is very similar to that of Ce 3*d* spectra. It should be noticed that there is an appearance of small $4f^0$ features for a 1.5-ML film. For greater thicknesses, their intensity increases, reaches a maximum for 2.5-ML, and then decreases. One can also observe that Fe 3*s* intensity decreases continuously with cerium deposition and becomes nearly zero for a 8-ML film. This behavior qualitatively confirms the absence of any interdiffusion that would lead to the persistence of the iron signal.

The formation of a strongly hybridized cerium phase at the interface with iron has already been reported in the case of Ce/Fe multilayers.[21] In that case, iron layers were polycrystalline and strongly (110) textured in the layer plane for thicknesses greater than 25 Å. We were then interested in the

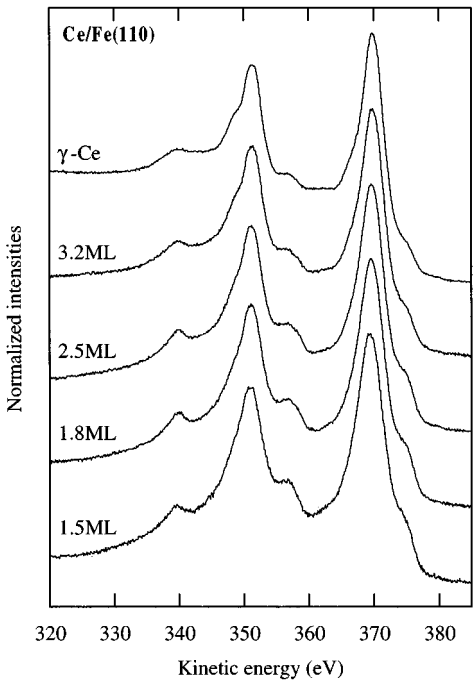

FIG. 5. Ce 3*d* photoemission spectra for different cerium thicknesses on Fe(110). All spectra are normalized at the $4f^1$ feature intensity at 369 eV.

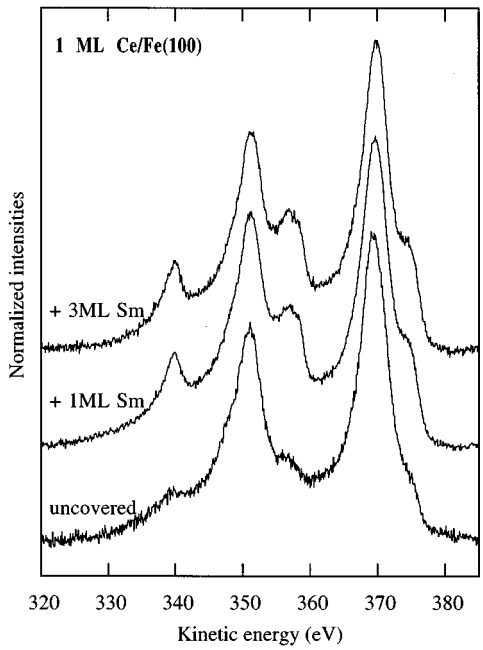

FIG. 6. Ce 3*d* photoemission spectra for one monolayer of cerium covered with one and three monolayers of samarium and uncovered. The inelastic background has been subtracted by Shirley's method and the spectra are normalized at the $4f^1$ feature intensity at 369 eV.

influence of the iron surface orientation on cerium hybridization since (110) planes are denser than the (100) ones. For this purpose we have reproduced our experiments with (110) iron surfaces and the Ce 3*d* photoemission spectra are presented in Fig. 5. The evolution of the spectra is the same as in the case of the (100) surface. We can observe an increase in the $4f^0$ feature intensity, which reaches a maximum for a 2.5-ML film. For greater thicknesses, spectra look more and more like that of the γ-Ce phase. Moreover, the $4f^0$ feature intensities are roughly identical for a same thickness on the (100) or (110) iron surface. This result indicates that the symmetry and the compactness of iron surface do not greatly influence the electronic configuration of cerium at the interface.

IV. EXTRACTION OF THE CONTRIBUTIONS FROM THE DIFFERENT ATOMIC LAYERS AND SIMULATIONS

A. Cerium films with samarium coverage

As already mentioned, photoemission spectra for a few monolayer films correspond to an average of contributions from the various atomic layers that may have different electronic structures. It has been shown that some strongly hybridized cerium-based intermetallic compounds[14] or the α-Ce phase[16] exhibit a reduced hybridization at the surface. Thus, one may have to take into account the influence of this surface layer to obtain an accurate estimation of the cerium hybridization strength at the interface with iron.

In order to suppress the surface effect, we have prepared a one-cerium-monolayer film that has been covered with several layers of samarium. This samarium coverage is supposed to mimic the cerium presence on top of the cerium layer, which is in contact with the iron substrate and does not contribute to the Ce 3*d* photoemission spectrum. Indeed, 5*d* and 6*s* orbitals are very similar among the rare-earth series and samarium in the metallic state is trivalent as weakly hybridized cerium. We have checked by monitoring the evolution of Auger intensities with samarium coverage that no interdiffusion between cerium and samarium occurs at 130 K. The Ce 3*d* photoemission spectra for one cerium monolayer covered with three samarium monolayers is presented in Fig. 6. For comparison, one uncovered cerium monolayer spectrum is also shown.

The comparison of the two spectra is very impressive since the uncovered monolayer is trivalent whereas the covered monolayer exhibits a spectrum characteristic of a strongly hybridized phase. This spectrum presents $4f^0$ and $4f^2$ features that are much more intense than those observed for the various uncovered cerium films. This result unambiguously demonstrates that the cerium layer at the interface with iron is strongly hybridized if it is not affected by the surface effect.

This behavior also focuses on the importance of the free surface, which reduces the hybridization. One can, however, wonder if this effect is only restricted to the surface layer or if it affects several layers below the surface. To check this point, we have prepared a one-cerium-monolayer film covered with only one samarium monolayer. It should be noticed that the corresponding spectrum is only comparable to the other ones after Shirley-type background[36] subtraction. Indeed, the signal-to-background intensity ratio greatly depends on samarium coverage thickness: the three-samarium-monolayer coverage leads to a greater background level than in the one-monolayer coverage case. This behavior is due to the fact that Ce 3*d* photoelectrons have to travel through

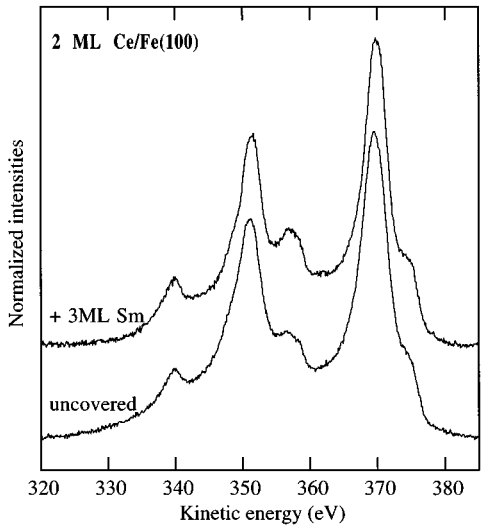

FIG. 7. Ce 3*d* photoemission spectra for two monolayers of cerium covered with three monolayers of samarium and uncovered. The inelastic background has been subtracted by Shirley's method and the spectra are normalized at the $4f^1$ feature intensity at 369 eV.

samarium and the probability that inelastic scatterings occur increases with increasing Sm thickness. One can see in Fig. 6 that the obtained spectrum is identical to the one observed with a three-samarium-monolayer coverage. One could then conclude that the surface hybridization reduction is restricted to the atomic layer that is at the surface.

We have also deposited a two-cerium-monolayer film covered by three samarium monolayers. The corresponding Ce 3*d* photoemission spectrum is compared in Fig. 7 to the two uncovered cerium monoloyers spectrum. As in the case of the one cerium monolayer, one can observe an enhancement of the $4f^0$ feature with the coverage. We have seen that the surface hybridization reduction only affects the first atomic layer. Consequently, for two covered or uncovered monolayer films, the cerium layer lying at the interface with iron has similar characteristics as the one covered monolayer. Then, the observed $4f^0$ feature enhancement for the covered film indicates that the second cerium layer is more hybridized than in the uncovered case. This results demonstrates that the iron substrate influence is also felt by the second cerium layer if it is not at the surface.

B. Contributions from the different atomic layers

From these results, we are now able to extract the contributions of each atomic layer from the different Ce 3*d* photoemission spectra. For instance, in the case of a three-cerium-monolayer film, the photoemission $S_{3\,\mathrm{ML}}$ spectrum contains three contributions: the S_1 contribution from the strongly hybridized interface cerium layer, the S_2 contribution from the less hybridized second layer, and the S_3 contribution from the trivalent surface layer. As we have already mentioned, inelastic background depends on the film thickness and it must be subtracted to allow comparison or combination of different spectra.

The S_1 contribution from the interface layer is simply given by $S_{1\mathrm{ML},c}$, the spectra of one covered monolayer:

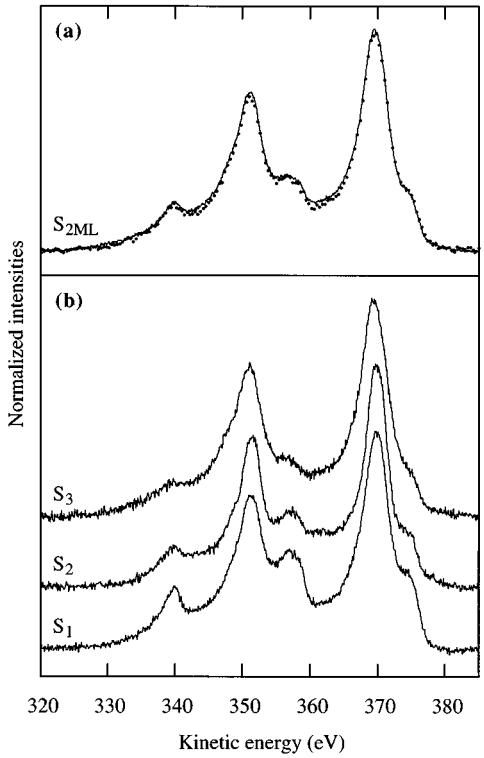

FIG. 8. (a) Background subtracted Ce 3*d* experimental spectrum (solid line) $S_{2\ \mathrm{ML}}$ and spectrum constructed (points) from S_1 and S_3 contributions (see text). (b) S_1, S_2, and S_3 contributions to the Ce 3*d* photoemission spectrum obtained for a three-monolayer cerium film.

$$S_1 = S_{1\ \mathrm{ML},c}\,. \tag{4.1}$$

The S_3 contribution from the surface layer is given by $S_{1\,\mathrm{ML}}$, the spectra of one uncovered monolayer:

$$S_3 = S_{1\ \mathrm{ML}}\,. \tag{4.2}$$

The contribution from the second layer (S_2) is obtained by subtraction of the S_1 contribution of the interface layer (attenuated by a coefficient C due to the electron attenuation length) from the $S_{2\,\mathrm{ML},c}$ spectrum obtained for a two-monolayer-covered cerium film:

$$S_{2\,\mathrm{ML},c} = \frac{CS_1 + S_2}{C+1}, \tag{4.3}$$

$$\Rightarrow S_2 = (1+C)S_{2\,\mathrm{ML},c} - CS_1\,. \tag{4.4}$$

Note that the area of all the spectra have to be normalized to unity.

The value of the $C = \exp(-d/\lambda)$ attenuation coefficient (where d is the equivalent thickness of one Ce or Sm monolayer and λ is the electron attenuation length at Ce 3*d* photoelectron energy) is obtained by reconstruction and fit of the $S_{2\,\mathrm{ML}}$ two uncovered monolayer spectra from the attenuated S_1 interface layer contribution and the S_3 surface layer contribution [Fig. 8(a)]:

$$S_{2\,\mathrm{ML}}=\frac{\exp(-d/\lambda)S_1+S_3}{\exp(-d/\lambda)+1}. \tag{4.5}$$

We then obtain a value of $C=0.6$ but it is not drastic: in the range $0.55<C<0.65$ (i.e., $4.6<\lambda<6.4$ Å), $S_{2\,\mathrm{ML}}$ experimental spectra constructed according to Eq. (4.5) still correspond to each other.

The S_1, S_2, and S_3 spectra are presented in Fig. 8(b).

C. Reconstruction of all experimental spectra

It is now possible to reproduce all the experimental Ce 3*d* spectra obtained for different thicknesses from four basic contributions: the S_1 contribution from the layer located at the interface, the S_2 contribution from the second layer, the $S_{\gamma\text{-Ce}}$ contribution of a γ-Ce phase (which corresponds to the layers located between the second layer and the surface), and the S_3 contribution from the surface layer.

The contribution from a layer covered with n atomic planes is attenuated with a factor $C^n=\exp(-nd/\lambda)$ and then we get the expression of the reconstructed spectra for all cerium layer thicknesses:

$$S_{1\ \mathrm{ML}}=S_3, \tag{4.6}$$

$$S_{1.5\ \mathrm{ML}}=\frac{0.5CS_1+S_3}{0.5C+1}, \tag{4.7}$$

$$S_{2\ \mathrm{ML}}=\frac{CS_1+S_3}{C+1}, \tag{4.8}$$

$$S_{2.5\ \mathrm{ML}}=\frac{0.5(C^2+C)S_1+0.5CS_2+S_3}{0.5C^2+C+1}, \tag{4.9}$$

$$S_{4\ \mathrm{ML}}=\frac{C^3S_1+C^2S_2+CS_{\gamma\text{-Ce}}+S_3}{C^3+C^2+C+1}, \tag{4.10}$$

and generalizing:

$$S_{n\ \mathrm{ML}}=\frac{C^{n-1}S_1+C^{n-2}S_2+\Sigma_{i=1}^{n-3}C^iS_{\gamma\text{-Ce}}+S_3}{\Sigma_{i=1}^{n-1}C^i+1}. \tag{4.11}$$

The obtained spectra are shown in Fig. 9 and it should be again noticed that calculated and experimental spectra still correspond to each other for $0.55<C<0.65$.

Using the S_3 spectrum for the contributions from the bulk trivalent layers instead of $S_{\gamma\text{-Ce}}$ would lead to the same agreement of the $4f^0$ and $4f^2$ features evolution with the experimental data. Nevertheless, the use of the $S_{\gamma\text{-Ce}}$ spectrum permits us to reproduce in addition the shoulder that appears at 348 eV on the $4f^1\ 3d_{3/2}$ feature.

It should be noticed that this analysis remains valid even if a multilayer growth occurs after four monolayers since the cerium is trivalent above three monolayers.

D. Calculation of the single-atomic-layer contributions

In order to get semiquantitative information about electronic structure of cerium atoms near the interface with iron, we have numerically simulated the spectra of the different contributions discussed in Sec. IV B in the framework of the

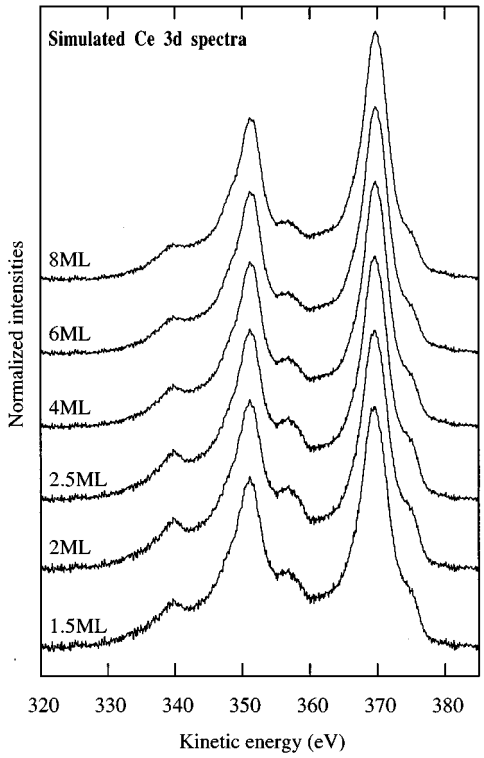

FIG. 9. Simulated Ce 3*d* photoemission spectra obtained by combination of four contributions (see text) for different cerium thicknesses.

Gunnarsson-Schönhammer Hamiltonian. This model gives an extension of the Anderson Hamiltonian[37] to describe the core-level spectroscopies. To take into account the effect of the core hole, the Hamiltonian is modified in the final state according to[38]

$$H_{GS}=H_0-U_{fc}\sum_{m,\sigma} n_{m,\sigma}+\varepsilon_c, \tag{4.12}$$

where:

$$H_0=\sum_{k,\sigma}\varepsilon_k a_k^\dagger a_k+\sum_{m,\sigma}\varepsilon_f a_{m,\sigma}^\dagger a_{m,\sigma}+\frac{U_{ff}}{2}\sum_{\substack{m,\sigma\\ m',\sigma'}} n_{m,\sigma}n_{m',\sigma'}+\sum_{k,m,\sigma}(V_{k,m}a_{m,\sigma}^\dagger a_k+\mathrm{H.c.}) \tag{4.13}$$

is the one impurity Anderson Hamiltonian.

The parameters of the model are as follows: ε_f is the energy of the $4f$ states; V is the hybridization between $4f$ and conduction states; U_{ff} is the Coulomb interaction between $4f$ electrons; and U_{fc} is the Coulomb interaction between $4f$ states and the core hole in the final state.

We have used an approach proposed by Kotani and co-workers[39,40] which is based on a direct diagonalization of the Hamiltonian H_{GS} in a restricted basis. In our calculation, the conduction band is rectangular and discretized in 20 equidistant states.

The obtained spectra are convoluted with a 1-eV full width at half-maximum (FWHM) Lorentzian in order to take

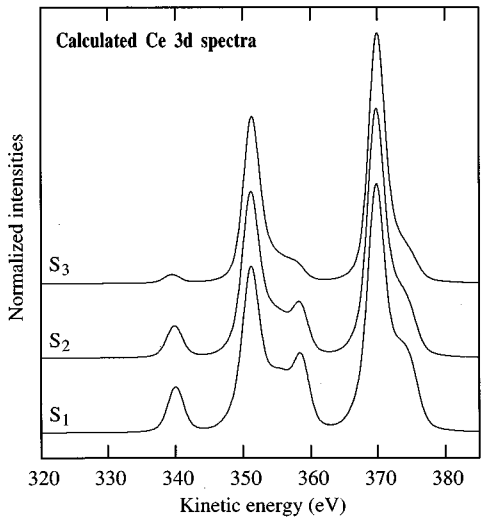

FIG. 10. Ce 3*d* photoemission spectra calculated with Gunnarsson-Schönhammer's model to simulate S_1, S_2, and S_3 contributions (see text).

into account the finite core-hole lifetime and with a 2.2-eV FWHM Gaussian simulating the experimental resolution and multiplet effect broadenings. The calculated spectra obtained for describing the S_1, S_2, and S_3 contributions discussed in Sec. IV B are shown in Fig. 10. Although these calculated spectra are in a rather good qualitative agreement with the spectra of Fig. 8, they do not exactly reproduce them because the model does not consider multiplet effects. Our aim was only to reproduce intensities of the $4f^0$ and $4f^2$ features that reflect respectively the $4f$ state occupation and the hybridization strength in the initial state. The model parameters used are reported in Table I. For comparison, we add the parameters for the α-Ce spectrum from Ref. 35 without taking into account a surface contribution. It should be noticed that the hybridization of the interface layer S_1 is larger than the value obtained for the α-Ce phase while the $4f$ state occupation number is smaller. This result indicates that the α-Ce phase is certainly much more hybridized than it is generally considered following a direct interpretation of photoemission spectra that contain a surface contribution. The second layer S_2 is less hybridized but still feels the iron influence since its parameters compare to those of the α-Ce phase when the surface is not taken into account. Finally, the surface layer S_3 is found to be γ-like with a $4f$ states occupation number of about one. The position of its $4f$ states is shifted toward higher binding energies compared to bulk value as it has been already found.[8]

TABLE I. Gunnarsson-Schönhammer model parameter values used to obtain S_1, S_2, and S_3 spectra of Fig. 10 and α-Ce spectrum of Ref. 35.

	First atomic layer (S_1)	Second atomic layer (S_2)	Surface layer (S_3)	α-Ce
U_{ff} (eV)	6.8	6.8	6.8	6.8
U_{fc} (eV)	10.5	10.5	10.5	10.5
ε_f (eV)	-1.2	-1.2	-1.5	-1.2
V (eV)	0.355	0.315	0.260	0.320
n_f	0.818	0.861	0.964	0.855

V. CONCLUSION

A room-temperature study of the electronic properties study of Ce/Fe interfaces has been presented. The cerium growth is two dimensional and the interface is sharp without noticeable interdiffusion. The cerium films do not exhibit long-range order. For thicknesses greater than 2 ML, photoemission results reveal that cerium $4f$ states are strongly hybridized at the interface with iron states for cerium films deposited on both Fe(100) and Fe(110) surfaces. Therefore, symmetry and compactness of the iron surface do not affect this cerium behavior. In the case of films thinner than two monolayers, the cerium hybridization is strongly reduced by the free surface. By covering these films with a few samarium layers, we have suppressed the contact with the surface and then directly obtained the photoemission spectrum of interface cerium atoms. This original method has permitted us to confirm the crucial role played by the free surface, which strongly reduces the hybridization at the surface of α-like systems. On the other hand, photoemission spectra then obtained are representative of the bulk electronic structure without numerical treatment so as to subtract a surface contribution. We have also demonstrated unambiguously that this surface hybridization reduction only affects the first atomic layer.

The photoemission contributions from every atomic layer with different electronic structures have been separated. All experimental spectra can then be reconstructed from four basic contributions: contributions from the two strongly hybridized cerium layers at the interface, the contribution from the weakly hybridized surface layer and a contribution of γ-Ce due to all the intermediate cerium layers for larger thicknesses.

The contributions from interface layers and surface layer have been calculated in the Gunnarsson-Schönhammer model framework. The hybridization of the interface layer is found to be stronger than that of the α-Ce phase if the surface contribution is not considered. We can then conclude that one must take into account the surface contribution in order to perform a correct interpretation of photoemission results obtained on α-like Ce systems. This procedure of coverage by a rare-earth overlayer could be used in the future in order to get directly the bulk photoemission contribution of many α-like Ce systems.

ACKNOWLEDGMENTS

We wish to acknowledge S. Andrieu, Ph. Arcade, and M. Piecuch for the fabrication of the iron monocrystalline substrates.

*Laboratoire de Physique du Solide is Unité de Recherche Associée 155 au Centre National de la Recherche Scientifique.

[1] D.C. Koskenmaki and K.A. Gschneidner, Jr., in *Handbook on the Physics and Chemistry of Rare Earths*, edited by K.A. Gschneidner, Jr. and L. Eyring (North-Holland, Amsterdam, 1978), Vol. 1, p. 337.

[2] D. Glötzel, J. Phys. F **8**, L163 (1978).

[3] W.E. Pickett, A.J. Freeman, and D.D. Koelling, Phys. Rev. B **23**, 1266 (1981).

[4] L. Severin and B. Johansson, Phys. Rev. B **50**, 17 886 (1994).

[5] B. Johansson, Philos. Mag. **30**, 469 (1974).

[6] P. Coleman, Phys. Rev. B **29**, 3035 (1984).

[7] N.E. Bickers, D.L. Cox, and J.W. Wilkins, Phys. Rev. Lett. **54**, 230 (1985); Phys. Rev. B **36**, 2036 (1987).

[8] L.Z. Liu, J.W. Allen, O. Gunnarsson, N.E. Christensen, and O.K. Andersen, Phys. Rev. B **45**, 8934 (1992).

[9] G.K. Wertheim and G. Crecelius, Phys. Rev. Lett. **40**, 813 (1978).

[10] B. Johansson, Phys. Rev. B **19**, 6615 (1979).

[11] C. Laubschat, B. Perscheid, and W.-D. Schneider, Phys. Rev. B **28**, 4342 (1983).

[12] C.L. Nicklin, C. Binns, C. Norris, E. Alleno, and M.-G. Barthés-Labrousse, Surf. Sci. **307-309**, 858 (1994).

[13] O. Eriksson, R.C. Albers, A.M. Boring, G.W. Fernando, Y.G. Hao, and B.R. Cooper, Phys. Rev. B **43**, 3137 (1991).

[14] C. Laubschat, E. Weschke, C. Holtz, M. Domke, O. Strebel, and G. Kaindl, Phys. Rev. Lett. **65**, 1639 (1990).

[15] E. Weschke, C. Laubschat, R. Ecker, A. Höhr, M. Domke, G. Kaindl, L. Severin, and B. Johansson, Phys. Rev. Lett. **69**, 1792 (1992).

[16] E. Weschke, C. Laubschat, T. Simmons, M. Domke, O. Strebel, and G. Kaindl, Phys. Rev. B **44**, 8304 (1991).

[17] J. Tang, J.M. Lawrence, and J.C. Hemminger, Phys. Rev. B **48**, 15 342 (1993).

[18] C. Gu, X. Wu, C.G. Olson, and D.W. Lynch, Phys. Rev. Lett. **67**, 1622 (1991).

[19] L. Braicovich, L. Duó, P. Vavassori, and G.L. Olcese, Surf. Sci. **331-333**, 782 (1995).

[20] F. Klose, M. Steins, T. Kacsich, and W. Felsch, J. Appl. Phys. **74**, 1040 (1993).

[21] F. Klose, O. Schulte, F. Rose, W. Felsch, S. Pizzini, C. Giorgetti, F. Baudelet, E. Dartyge, G. Krill, and A. Fontaine, Phys. Rev. B **50**, 6174 (1994).

[22] M. Finazzi, F.M.F. de Groot, A.-M. Dias, B. Kierren, F. Bertran, Ph. Sainctavit, J.-P. Kappler, O. Schulte, W. Felsch, and G. Krill, Phys. Rev. Lett. **75**, 4654 (1995).

[23] S. Andrieu, M. Piecuch, H. Fischer, J.F. Bobo, F. Bertran, Ph. Bauer, and M. Hennion, J. Magn. Magn. Mater. **121**, 30 (1993).

[24] S. Andrieu, M. Piecuch, and J.F. Bobo, Phys. Rev. B **46**, 4909 (1992).

[25] T. Gourieux, B. Kierren, F. Bertran, D. Malterre, and G. Krill, Surf. Sci. (to be published).

[26] M.P. Seah and W.A. Dench, Surf. Interface Anal. **1**, 2 (1979).

[27] C.J. Powell, J. Electron Spectrosc. Relat. Phenom. **47**, 197 (1988).

[28] S. Tanuma, C.J. Powell, and D.R. Penn, J. Vac. Sci. Technol. A **8**, 2213 (1990); J. Electron Spectrosc. Relat. Phenom. **52**, 285 (1990); Surf. Interface Anal. **17**, 911 (1991).

[29] B. Kierren, F. Bertran, T. Gourieux, and G. Krill, J. Phys. Condens. Matter **6**, L201 (1994).

[30] M. Taborelli, R. Allenspach, G. Boffa, and M. Landolt, Phys. Rev. Lett. **56**, 2869 (1986).

[31] C. Carbone and E. Kisker, Phys. Rev. B **36**, 1280 (1987).

[32] C. Carbone, R. Rochow, L. Braicovich, R. Jungblut, T. Kachel, D. Tillmann, and E. Kisker, Phys. Rev. B **41**, 3866 (1990).

[33] E. Vescovo, R. Rochow, T. Kachel, and C. Carbone, Phys. Rev. B **46**, 4788 (1992).

[34] J.C. Fuggle, F.U. Hillebrecht, Z. Zołnierek, R. Lässer, Ch. Freiburg, O. Gunnarsson, and K. Schönhammer, Phys. Rev. B **27**, 7330 (1983).

[35] E. Wuilloud, H.R. Moser, W.-D. Schneider, and Y. Baer, Phys. Rev. B **28**, 7354 (1983).

[36] D.A. Shirley, Phys. Rev. B **5**, 4709 (1972).

[37] P.W. Anderson, Phys. Rev. **124**, 41 (1961).

[38] O. Gunnarsson and K. Schönhammer, Phys. Rev. B **28**, 4315 (1983).

[39] T. Nakano, A. Kotani, and J.C. Parlebas, J. Phys. Soc. Jpn. **56**, 2201 (1987).

[40] A. Kotani, T. Jo, and J.C. Parlebas, Adv. Phys. **37**, 37 (1988).